Acoustic anomalies in $Tb_2(MoO_4)_3$ and the "missing" A_1 optic mode

P. A. Fleury, K. B. Lyons, and R. S. Katiyar*
Bell Laboratories, Murray Hill, New Jersey 07974
(Received 22 March 1982; revised manuscript received 7 September 1982)

Anomalies in both the acoustic- and optic-phonon spectra associated with the ferroelectric and ferroelastic phase transition in terbium molybdate have been quantitatively measured by simultaneous Brillouin and Raman spectroscopy. The most striking singular behavior observed is the divergent damping of both the A_1 optic phonon and the C_{11} acoustic phonon upon approach to T_0 from below. T_0 was determined to be 159 °C for our sample by measurement of the pyroelectric response. The A_1-mode frequency determined from the Raman spectrum shows little temperature dependence, while the C_{11} elastic constant determined from the Brillouin spectra decreases by about 60% between room temperature and T_0. There is no evidence of a dynamic central peak. The observed anomalies in the acoustic velocity and damping are incompatible with a model based on bilinear coupling between the acoustic mode and the A_1 mode seen in the Raman spectrum. However, a satisfactory account of all the experimental observations (including the anomalies in $\tilde{C}_{11}$ and C_{22}) can be obtained by assuming the presence of a second A_1 optic phonon with a negligible Raman scattering cross section. We note that the dynamic variables below T_0 are not simply related to the distortion, as has often been assumed previously. On the basis of this model we use the acoustic velocities and damping to determine the frequency and damping parameters of this unseen mode. It is emphasized that the singular behavior of the damping of the observed A_1 mode has yet to receive adequate theoretical explanation.

I. INTRODUCTION

Since the discovery of ferroelectricity[1] and the unusual associated elastic and dielectric behaviors[2] in the rare-earth-metal molybdates sustained attention has been given to the dynamical aspects of the phase transition with often confusing or apparently contradictory results. X-ray[3] and neutron[4] scattering have established that in $Tb_2(MoO_4)_3$ and $Gd_2(MoO_4)_3$ (referred to hereafter as TMO and GMO, respectively) the transition from the paraelectric D_{2d}^3 phase to the ferroelectric and ferroelastic C_{2v}^8 phase occurs at $T_0 \approx 160$ °C, is weakly first order, involves a doubling of the tetragonal unit cell, and is associated with a doubly degenerate soft optic phonon at the M point of the tetragonal Brillouin zone. Although this mode is expected on group-theoretical grounds to give rise below T_0 to two A_1 symmetry soft modes, Raman,[5] infrared,[6] and neutron[4] observations have not borne out such simple expectations. In particular, although at temperatures below ≈ 0 °C two A_1 components are resolved[6–8] (at 44 and 49 cm^{-1}), the evolution of the spectra between room temperature and T_0 is dominated by an extreme broadening (and complete indistinguishability) of these components with little evident softening of the frequency parameters. Furthermore, the several attempts to account for the observed[9–13] acoustic-phonon behavior in terms of bilinear coupling with the optic phonons have not been quantitatively or sometimes even qualitatively successful. Some of these attempts have involved widely differing assumptions about the frequency and temperature dependence of the so called "missing mode"—i.e., the companion to the broad A_1 feature 47 cm^{-1}. These range from assuming that it remains degenerate in both frequency and damping with the observed Raman mode to postulating that it lies at very low frequencies and might be responsible for the unresolved central peak observed in neutron scattering and inferred from some Raman experiments.

Yao *et al.*[14] have made the most thorough attempt to date to explain the acoustic behavior, using models encompassing all these possibilities, and have concluded that, while it is possible to fit $\tilde{C}_{11}$ alone, the behavior of C_{22} and C_{11} is not simultaneously consistent with any of their models. We have modified their approach, particularly as regards the orientation of the normal-mode eigenvectors with

respect to that of the distortion, and we show below that it is in fact possible to fit all the available acoustic and Raman data in the context of a model invoking a linear coupling with an "unseen" mode.

II. EXPERIMENTAL PROCEDURE

The experiments reported here on TMO were conducted in order to (1) provide a definitive search for the missing mode down to previously inaccessible low frequencies (≈ 0.02 cm^{-1}), (2) measure carefully both the frequencies and lifetimes of the A_1 optic phonon and the appropriate acoustic phonon over the temperature range between 25 and 180 °C, and (3) elucidate the existence and dynamic characteristics, if any, of the central peak. The experimental procedure involved simultaneous measurements of Raman and Brillouin spectra (using a double-grating spectrometer and a tandem Fabry-Perot interferometer, respectively, both with a molecular-iodine reabsorption cell to remove elastically scattered light) together with *in situ* measurement of the pyroelectric coefficient. The resonant reabsorption of elastically scattered light with a molecular-iodine filter completely removed stray light from all the spectra. As described in detail elsewhere[15] all spectra were corrected through the use of computer-assisted normalization procedures for distortions imparted by subsidiary iodine absorptions. The pyroelectric coefficient was measured by using the chopped (1-kHz) laser beam itself to heat the crystal periodically in times (with peak-to-peak temperature modulation of a few millidegrees) and measuring the amplitude of the voltage thus induced across the sample. As shown in Fig. 1., when the sample is uniformly illuminated with 5145-Å light from an unfocused laser beam, the pyroelectric responses agree very well with earlier measurements, and provide an accurate determination of T_0 in our TMO sample ($T_0 = 159.0$ °C). With the beam focussed to 100-μm diameter, as in the spectroscopic runs, the pyroelectric response shows two differences. First, the main peak is broadened and diminished, reflecting the existence within the scattering volume of a steady-state laser-induced temperature smearing of 1–2 °C. The consequences of this for the Brillouin spectra very near T_0 will become evident below. Second, a much weaker secondary maximum at an apparent temperature of 162 °C is associated with an approximately 3-°C difference in temperature between the scattering volume and the unilluminated bulk of the crystal. This local heating (induced by ~ 70 mW of 5145-Å light in our experiments) is associated with absorptions of the Tb^{3+} and is more severe at other wavelengths or higher powers. Its effects are thus expected to be present in any Raman or Brillouin spectra of TMO, although they will be negligible except very near T_0.

It should be noted that absorption of 5145-Å light may produce excited-state dipoles in significant numbers in TMO. Depending upon the lifetimes of such excited states, the associated internal electric fields could in principle affect both the static and dynamic ferroelectric behavior near T_c. Relatively long-lived optically excited polarization fields have been studied, for example, in $BaMnF_4$.[16] Our observations in TMO indicate that the thermal effects of optical absorption dominate any exciton-related dipolar effects, but more experiments would be required to assess the latter quantitatively.

III. RESULTS

The Raman spectra, shown in Fig. 2, are obtained in the $x(zz)y$ geometry (where the A_1 modes are active) with 100-μm slits, using an iodine cell to remove completely any light whose frequency lies

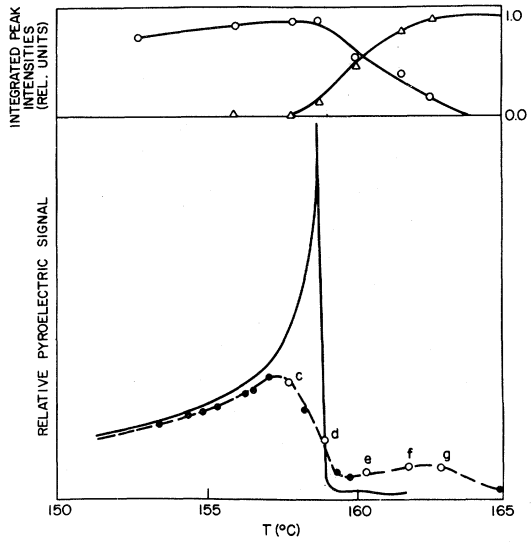

FIG. 1. Pyroelectric response in TMO vs temperature using chopped 5145-Å laser beam for heating. Lower portion: solid curve from uniform illumination of entire sample volume; dashed curve focused (100-μm) beam. Open circles labeled $a-h$ represent the temperatures at which the spectra shown in Fig. 5, labeled correspondingly, were taken. Upper portion: circles and triangles represent integrated intensities of LA Brillouin peaks corresponding to ferroelectric and paraelectric phases, respectively.

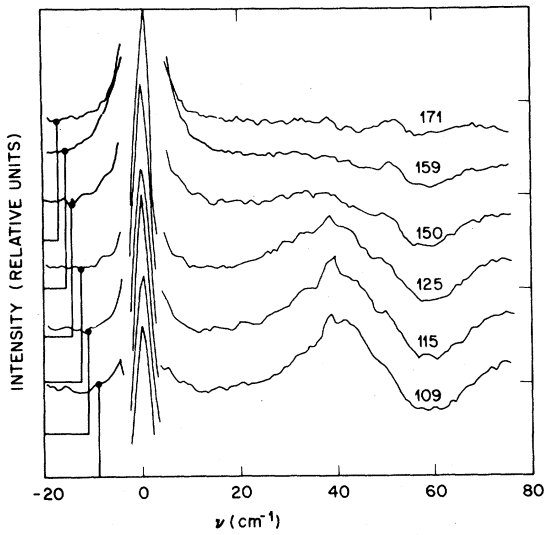

FIG. 2. Raman spectra of TMO taken with ~ 100-μm slits and an iodine-absorption cell to eliminate elastic scattering. Unresolved structure centered about zero-frequency shift is reduced 100× for display. Structure induced by the iodine cell has been removed by computer analysis (Ref. 15) but some remnants of this structure exacerbate the apparent noise, which is also increased in comparison to previously reported spectra due to low laser power (70 mW) and high resolution. Note the relatively intense featureless multiphonon background evident in all spectra, including that at 171 °C. Baseline appropriate to each spectrum is indicated on the left.

within ± 0.015 cm^{-1} of the 5145-Å single-mode laser frequency. Between ~ 25 and ~ 100 °C the A_1 mode at 47 cm^{-1} is fairly well defined, although significant broadening is evident as the temperature is increased. There are three aspects of Fig. 2 which deserve comment. First, notice the substantial, broad flat background (which equals or exceeds the A_1 peak intensity at 142 °C and higher) due to multiphonon processes, which remains essentially unchanged above T_0. Particularly above ~ 140 °C this background, in combination with the extreme broadening of the A_1 phonon mode, introduces substantial correlation between the frequency and linewidth parameters extracted for this mode. Second, the unresolved central peaks, shown here attenuated by a factor of 100 are entirely inelastic since the iodine cell has been used. The Fabry-Perot spectra to be discussed below reveal the detailed spectral profile for frequencies below 1 cm^{-1}. For the moment, it is important merely to notice that neither the central intensity nor the associated tail extending out to 5—10 cm^{-1} exhibits singular behavior near T_0.

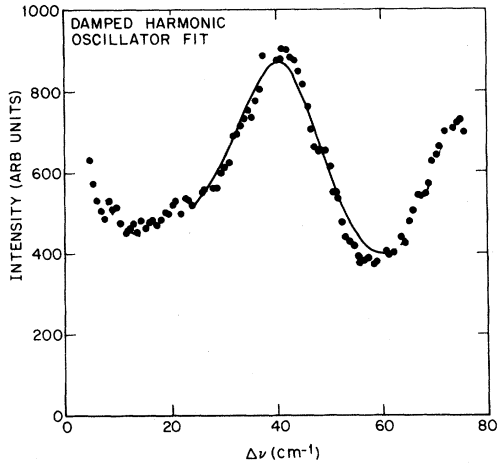

FIG. 3. Damped-harmonic-oscillator fit (solid curve) to the Raman spectrum (solid dots) at 97 °C.

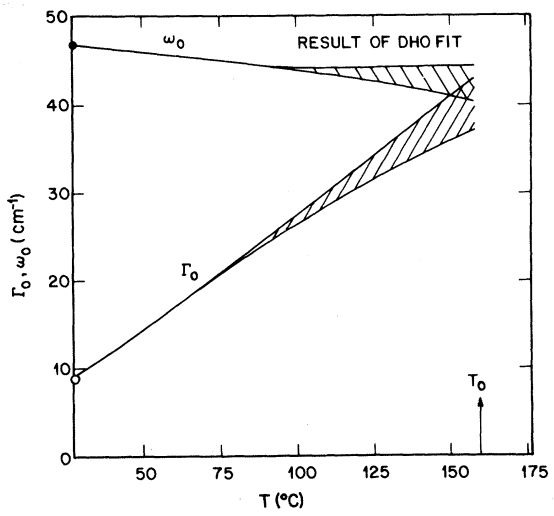

FIG. 4. Temperature dependence of the optic-phonon damped-harmonic-oscillator parameters, ω_0 and Γ_0. Shaded areas represent temperatures for which ω_0 and Γ_0 are strongly correlated in these fits.

Figure 3 shows a typical fit to the Raman spectrum using the damped-harmonic-oscillator model. From this and similar spectra values of the optic-mode frequency and damping parameters, ω_0 and Γ_0, are extracted and displayed in Fig. 4. Although the correlation renders the separate values somewhat uncertain within ~ 30 °C of T_0, the observed behavior is well described by assuming that ω_0 is nearly temperature independent (~ 45 cm^{-1}), while T_0 increases strongly near T_0. As expected, there is no evidence of A_1-mode scattering above T_0.

Examination of the low-frequency portions of these spectra under the high resolution achievable with the tandem Fabry-Perot reveals spectra shown in Fig. 5. Here the scattering wave vector, $\vec{q}$, lies

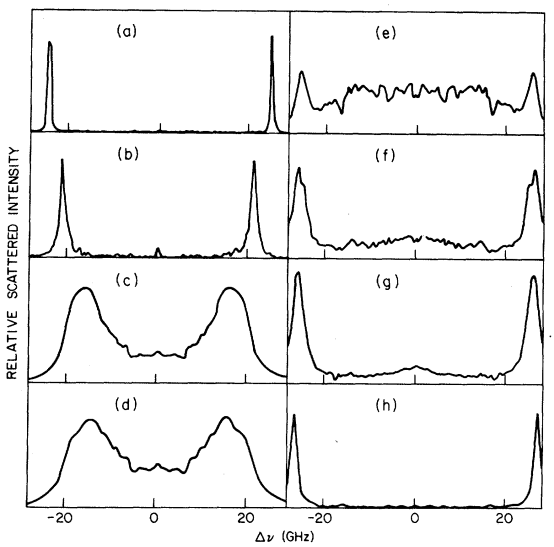

FIG. 5. Brillouin spectra of LA phonons propagating along ferroelectric x axis, obtained using tandem Fabry-Perot in conjunction with iodine-absorption cell to remove completely the elastic component. Structure induced by the iodine cell has been removed by computer analysis. Scattering volume temperatures are (a) 25 °C, (b) 125 °C, (c) 158 °C, (d) 159 °C, (e) 160.2 °C, (f) 162 °C, (g) 163 °C, and (h) 170 °C. Note in (e)–(g) the coexistence of both para- and ferroelectric phase Brillouin features.

nearly parallel to the ferroelectric [100] direction and the scattering angle is $\theta=135°$. These are polarized spectra so that we are examining longitudinal-acoustic phonons whose frequencies are determined by the C_{11} elastic constant where $C_{11}=\rho(\omega_a^2/q^2)$, with $\rho=4.64$ g/cm^3, $q=4(\pi/\lambda)n\sin\theta/2$, $n=1.906$, $\lambda=5145$ Å, and $\theta=135°$. These spectra are fit adequately by a damped-harmonic-oscillator function, shown for a typical example in Fig. 6. The parameters from these fits are shown in Fig. 7. Note that both the width and the frequency parameters may be unambiguously extracted from our data.

Between 25 and 150 °C the spectra are fully characterized by the softening and gradual broadening of the Brillouin peaks. Very close to T_0 (≥ 153 °C) the rate of broadening increases significantly. This evolution continues to proceed smoothly up to at least within ~ 1 °C of T_0. The spectra with indicated temperatures between 160 and 163 °C appear at first glance to exhibit a broad ~ 20 GHz) central peak coexisting with a well-defined Brillouin doublet at ± 26.2 GHz. Careful study of this temperature regime using various laser powers, however, has revealed that this spectral appearance is a consequence of the temperature smearing within the scattering volume described earlier. That is, different parts of the scattering volume are simultaneously above and below T_0. The central component is merely the overdamped Brillouin doublet for $T \leq T_0$, whereas higher-frequency doublet comes from those portions of the scattering volume where $T \geq T_0$. Further confirmation of this result is provided by the upper portion of Fig. 1 where the integrated intensities of these two types of features are displayed for various temperatures.

The quantitative measurements of the width of the Brillouin components provided by our spectra

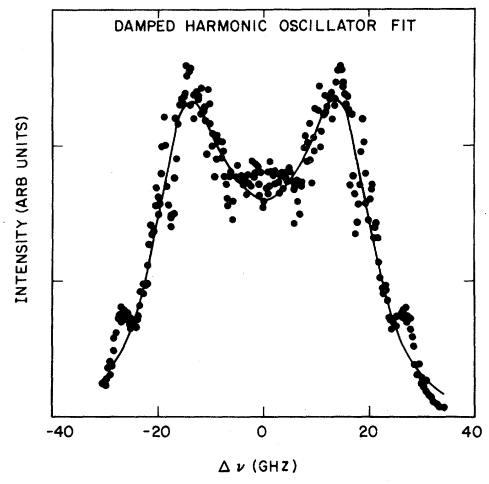

FIG. 6. Damped-harmonic-oscillator fit (solid curve) to Brillouin spectrum near T_0 ($T=157$ °C). No provision was made in the fitting for temperature smearing within the scattering volume.

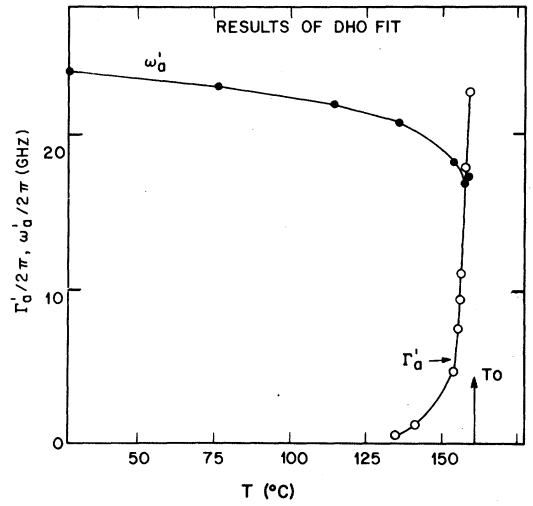

FIG. 7. Temperature dependence of acoustic-phonon damped-harmonic-oscillator parameters ω_a' and Γ_a' obtained from fits such as displayed in Fig. 6.

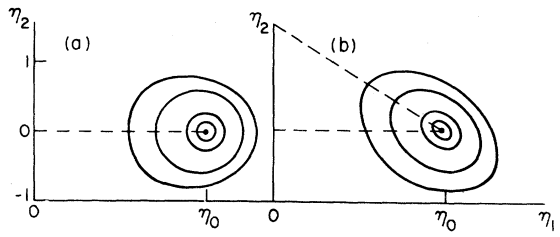

FIG. 8. Equipotential curves in the (η_1,η_2) plane for the free energy of Dorner *et al.*,[4] rotated so that $\eta_{20}\equiv 0$, for $W_3'=0$ [part (a)] and for $\tan 2\psi=(3B_3+5W_3\eta_0^2)/(B_2+2W_2\eta_0^2)$. Dashed lines indicate the expected orientations of the ellipse for the two cases, and [in part (b)] the line $\eta_2=0$.

exhibit a rather striking anomaly just below T_0. This anomaly parallels that in the optic mode revealed in the Raman spectrum. The latter exhibits a curious reversal of the usual behavior near a structural phase transition manifesting its critical behavior mainly in its width rather than in its frequency parameter. We shall have more comment about this relationship below.

IV. DISCUSSION AND CONCLUSIONS

The main observations from the high-resolution spectra are then (1) the C_{11} elastic constant softens in accord with previous reports,[9–13,17,14] (2) the acoustic-phonon damping is strongly singular (more so than previously reported) and results in overdamping of the acoustic mode within a degree or two of T_0, (3) there is no evidence of a dynamic central peak associated with critical fluctuations or relaxing phonon self-energies, etc., near T_0, (4) the spectral shapes at all temperatures can be fit well with the damped-harmonic-oscillator model using the values for ω_a' and Γ_a' displayed in Fig. 7.

We shall now discuss the compatibility of our Raman and Brillouin observations with existing coupled-mode theories for the TMO transition dynamics. Essentially all of the theoretical speculation and experimental interpretation involving the dynamics of the improper ferroelastic transition in the molybdates has been concerned with the fundamental anharmonic interaction between one acoustic and two "soft" optic phonons. Phenomenologically, this interaction enters the free energy through a term of the form $G_{\rm int}=-\frac{1}{2}K\epsilon\eta^2$, where ϵ and η represent, respectively, the dimensionless-strain (acoustic-mode) and order-parameter (optic-mode) amplitudes, and K the coupling coefficient. The same physical process can of course be described in a microscopic formulation involving the acoustic- and optic-phonon Green's functions and self-energies. Various theoretical[18–20] and experimental[12,14] paper have treated this interaction on various levels and with varying degrees of approximation. A particularly clear and tractable discussion of this formalism has been provided by Levanyuk.[20] Its application to TMO has been given by Yao *et al.*[14] We shall adopt the spirit of this approach here, with some differences, as discussed further below.

The free energy describing the TMO system has been written down by various authors,[4,14,19] in essentially equivalent fashion. Perhaps the most instructive notation to begin with is that of Dorner *et al.*[4] They write the free energy F as a function of the parameters η, γ_1, and γ_2 where η is the absolute value of the order parameter and its two components are $\eta\gamma_i$ for a given choice of coordinates. As they note, it is possible to rotate the axes in the xy plane without changing the functional form of their expression [their Eq. (10)]. They choose axes such that $\gamma_1=1$ and $\gamma_2=0$. However, it is important to remember that *below* the transition, such rotation is impermissible, and, in fact, the two normal modes of the soft-mode branch are determined unambiguously by the symmetry of the free-energy minimum. If we use their choice of coordinate axes, and expand the free energy about the point $(\eta_0,0)$ representing the static distortion in those coordinates, it is easily shown that the normal-mode eigenvectors are tilted with respect to those axes by an angle ψ defined (in their notation) by

$$\tan 2\psi=\frac{(3B_3+5W_3\eta_0^2)}{(B_2+2W_2\eta_0^2)}\ ,$$

as discussed in the Appendix and illustrated in Fig. 8. Thus, their static variables do not coincide with the dynamic variables below T_0.

In order to avoid this confusion, we prefer to *define* our coordinate axes above T_0 to be parallel to the eigenvectors of the soft-mode branches below T_0. In this case, it is obvious as a corollary to the statement above that the static displacement will not lie along either of the order-parameter axes.[19] Thus, in general the order parameter has the form $(\eta\sin\phi,\eta\cos\phi)$, and the static displacement is defined as $(\eta_0\sin\phi_0,\eta_0\cos\phi_0)$. Using this coordinate transformation, we obtain the free energy as written by Yao *et al.*,[14] in which the portion relevant to the interaction of the modes considered here takes the form

$$G_{\rm int}=\tfrac{1}{2}K_2\eta^2(\tilde{\epsilon}_1+\tilde{\epsilon}_2)+\tfrac{1}{2}\eta^2\tilde{\epsilon}_6(K_3\cos2\phi+K_4\sin2\phi)\ , \quad (1)$$

where $\tilde{\epsilon}_i$ are the strains referred to the axes characteristic of the paraelectric phase, and K_i are coupling constants. It must be emphasized that the expression above is valid for any choice of origin for ϕ, as noted by Dorner *et al.*[4]; however, our choice of coordinates differs from any used previously. In particular, the choice made in Eq. (3.16) of Yao *et al.*[14] is not *a priori* the same as ours. We shall see, however, that the two almost coincide accidentally. This corresponds to the statement that K_4 is nearly zero in our coordinate system. Below we give a plausibility argument for this condition.

It is now necessary to write Eq. (1) in terms of the strains of the ferroelectric phase, ϵ_i. This corresponds to a rotation of the *crystal* axes by 45°. (Note this has no effect on ϕ.) The transformation is easily carried out, and the relevant portion of the free energy becomes

$$G_{\rm int}=(K_2+K_3\cos2\phi+K_4\sin2\phi)\eta^2\epsilon_1+(K_2-K_3\cos2\phi-K_4\sin2\phi)\eta^2\epsilon_2\ . \quad (2)$$

Let us now expand this free energy around the equilibrium position, to obtain the coefficient of $\delta\eta_i\epsilon_1$. The coefficient for ϵ_2 will differ only in the sign of K_3 and K_4. Noting that not only must we expand η^2 but also the trigonometric terms $\cos2\phi$ and $\sin2\phi$, we obtain the coefficient for ϵ_1:

$$[(K_2+K_3)\sin\phi_0+K_4\cos\phi_0]\eta_0\delta\eta_1+[(K_2+K_3)\cos\phi_0-K_4\sin\phi_0]\eta_0\delta\eta_2\ . \quad (3)$$

From this, following the notation of Yao *et al.*,[14] we obtain the expression for C_{11} in the ferroelectric phase, taking into account only the morphically induced bilinear coupling terms:

$$C_{11}=C_{11}^0-\frac{[(K_2+K_3)\sin\phi_0+K_4\cos\phi_0]^2\eta_0^2}{m^*\Omega_1^2}-\frac{[(K_2+K_3)\cos\phi_0-K_4\sin\phi_0]^2\eta_0^2}{m^*\Omega_2^2}\ , \quad (4)$$

where $m^*=0.0461$ g/cm^2 is the effective mass for the optic mode,[14] the normal-mode frequency for the dynamic variable $\delta\eta_i$ is denoted Ω_i, and the order parameter is given by[4]

$$\eta_0^2(T)=\frac{\eta_0^2(T_0)}{3}[2+(160-T)^{1/2}] \quad (5)$$

(as in Ref. 14, we use $T_c=156$°C, in the notation of Ref. 4) where $\eta_0^2(T_0)=0.59\times10^{-16}$ cm^2. The expression for C_{22} is the same with the signs of K_3 and K_4 reversed. Note that here and in what follows we use $\Omega_{1,2}$ and $\Gamma_{1,2}$ to denote the theoretical soft-mode frequencies and dampings, to distinguish these quantities from the experimental values ω_0 and Γ_0 (Fig. 4), obtained from the Raman spectra, which probably represent some superposition of peaks. The various relationships among these quantities are discussed below.

For the case $\phi_0=\pi/2$ and $K_4=0$ the expression (4) reduces to that given by Yao *et al.*[14] While there is no reason to assume a special value of ϕ_0, there is a plausible reason that the value of K_4 should be small in our coordinate system. We have chosen coordinates such that the two order-parameter components $\eta_1=\eta_0\sin\phi_0$ and $\eta_2=\eta_0\cos\phi_0$ correspond to the dynamical variables below the transition. Thus, we could expect that the expansion of the free energy (2) about the equilibrium point should be an ellipsoid of revolution with its major axes along the coordinates. This requirement reduces to the condition $\partial^2G_{\rm int}/\partial\eta_1\partial\eta_2=0$. Since the only term in the free energy which is proportional to η_0^2 and which contains cross products of η_1 and η_2 is the term involving K_4 in (2), we conclude that that term must be small. While this argument is not rigorous, it does make it plausible that the value of K_4 should be small. In fact, we shall show below that a reasonable description of all the data is possible with $K_4=0$. This means that our coordinates in fact coincide closely with those chosen by Yao *et al.*[14] using a very different criterion.

In addition to the morphically induced bilinear coupling considered above, there are also fluctuation terms which may contribute to the acoustic anomalies. A calculation of these effects requires knowledge of the soft-mode frequencies and damping factors for the soft-mode branch throughout the Brillouin zone. Although this information is not all available, some attempts have been made at approximate evaluation of the integrals involved.[11,14] These attempts all involve assumptions as to the dispersion and damping as a function of wave vector. Nevertheless, such an approach is necessary for the description of the acoustic data above T_0 since the fluctuations terms are the only ones contributing in that region. In this temperature region, satisfactory agreement has been obtained.[11,14] Yao *et al.*[14] have extended this analysis below T_0 as well, and have found that the fluctuation contribution is quite negligible in that region. Hence, we shall ig-

nore it in what follows.

We first consider whether the elastic constant data below T_0 may be described consistently within this model. The model outlined above provides expressions for the temperature dependences of $\tilde{C}_{11}$, C_{11}, and C_{22}. The parameters involved in these expression are K_2, K_3, K_4, ϕ_0, C^0_{11}, $\tilde{C}^0_{11}$, Ω_1, and Ω_2. Of these, the values of Ω_i are known at room temperature from Raman and ir data, and we shall take them both to be 44 cm^{-1}. We shall assume that one mode, Ω_2 is temperature independent, consistent with the observed A_1 Raman spectrum. Furthermore, the values of C^0_{11} and $\tilde{C}^0_{11}$ may be extracted from the available acoustic data[11,12] above T_0. The value of $\tilde{C}^0_{11}$ is available quite directly from the data, and the data of Höchli[12] and that of Yao *et al.*[14] are all consistent with the value $\tilde{C}^0_{11}=80.7\times10^{10}$ dyne/cm^2. The value of C^0_{11}, on the other hand, is available only rather indirectly from data above T_0, as the combination[12] $C^0_{11}=\frac{1}{2}(\tilde{C}^0_{11}+\tilde{C}^0_{12})+\tilde{C}^0_{66}$. The necessary data are available from Höchli, and yield a value of roughly 77.5×10^{10} dyne/cm^2, while the data of Yao *et al.*[14] for C_{11} above T_0 indicate a value of about 78.2×10^{10} dyne/cm^2. Since we found that the fit is extremely sensitive to this parameter, we shall allow it to vary somewhat in the fit. We attempt to describe the data assuming various behaviors for Ω_1.

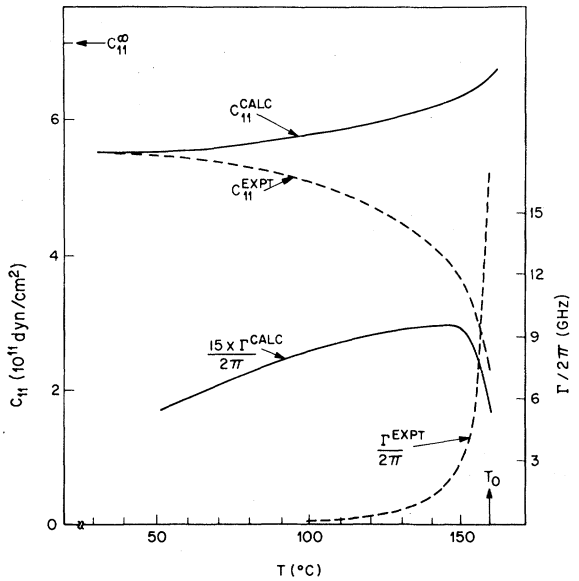

FIG. 9. Comparison of the experimental temperature dependences of the LA phonon damping (dashed curves) with the calculated results (solid curves) based on assuming that the unseen component is degenerate with that observed in the Raman spectrum. Value of the coupling constant has been determined at room temperature. Note the qualitative deviation of the curves for the elastic constant and the quantitative disagreement between the experimental and calculated Γ's.

If we assume that the missing mode Ω_1 is degenerate with the mode observed in the Raman spectrum, we find Ω_1 roughly independent of temperature. However, it is then not possible to describe the acoustic behavior. This is because the main temperature dependence in (4) then lies in η_0^2, and the calculated curve has the wrong slope as shown in Fig. 9. Therefore, we must allow Ω_1 to vary with T. Clearly, it would be possible to fit the observed behavior of C_{11} by allowing Ω_1 to assume any value required. In order to define the parameter values unambiguously, however, we may use the values of the other acoustic constants which are also given by the expressions above.

The second and more satisfactory procedure is then as follows. We begin by attempting to fit the data setting $K_4=0$. For a given value of C^0_{11} it is easy to solve for the values of K_2, K_3, and ϕ_0 which describe the room-temperature data for C_{11}, $\tilde{C}_{11}$, and C_{22}. We next use the value of $\tilde{C}_{11}$ at T_0 from Yao *et al.*[14] to determine the remaining parameter Ω_1. We then compare the resulting values of C_{11} and C_{22} with the data at T_0. By repeating this procedure for various values of C^0_{11} we find that the fit is extremely sensitive to the value chosen, mainly via the effect it has on the parameter ϕ_0. The value which best approximates the data at T_0 is $C^0_{11}=78.1\times10^{10}$ dyne/cm^2. This value lies within the range of the literature values indicated above. The other parameters chosen by this procedure are as follows: $K_2=0.454\times10^{26}$ dyne/cm^4, $K_3=-0.087\times10^{26}$ dyne/cm^4, and $\phi_0=76°$. A consistency check on these results can be made by using the relation given by Yao *et al.*: $K_3\cos2\phi_0\eta_0^2=2\tilde{C}^0_{66}\tilde{\epsilon}_6$. At room temperature this gives a value of about 2.2 mrad for $\tilde{\epsilon}_6$, which is within some 30% of the value available in the literature.[21]

Given the parameter values chosen from the room-temperature data by the above procedure, we then use our data on C_{11} as a function of temperature to determine the temperature dependence of Ω_1. These values are shown in Fig. 10(a). Finally, we use these values of Ω_1 to calculate the behavior of $\tilde{C}_{11}$ and C_{22} predicted by our model, and compare these to the behavior found by Yao *et al.*[14] The agreement [Fig. 10(b)] is quite satisfactory at all temperatures. We note also that our value of K_2 is the same as that found by Yao *et al.* within experimental error, so that their analysis for the data

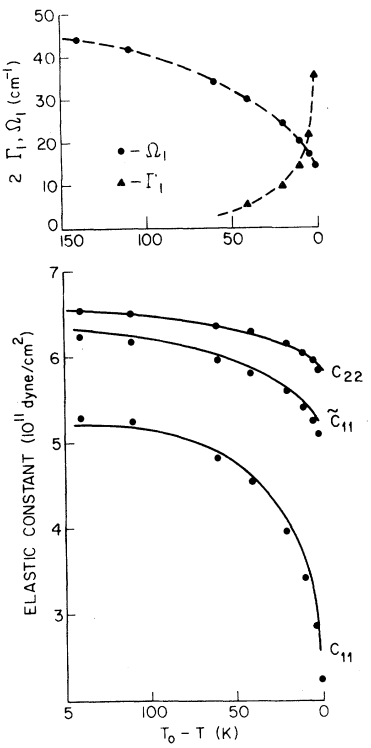

FIG. 10. Upper portion shows the soft-mode parameters which result from the model discussed in the text. Bottom shows the corresponding fit to the acoustic data for the three acoustic modes that show the strongest anomalies. Dashed lines are guides, solid lines show the experimental data of Yao *et al.* (Ref. 14), the points for C_{11} represent our data, and the points for the other two elastic constants represent calculations based on the model.

above T_0 would be unchanged.

The parametrization of the data given above seems to work quite well, However, there is one disturbing aspect of this situation which requires careful discussion. First, the portion of the free energy which governs the fluctuations of the order parameter[4] does not predict a soft-mode behavior below T_0 which remotely resembles that shown in Fig. 10(a). Furthermore, there is no independent experimental evidence for such a soft-mode behavior. Indeed, although two modes near 44 cm^{-1} may be resolved below 0 °C, and extension of this analysis to higher temperatures yields mode parameters which indicate some mode softening [8]; fits describing the Raman spectra equally well are possible using a single strongly-damped-harmonic-oscillator function with a frequency parameter quite independent of temperature.[5] Hence, the parameters resulting from a two-mode analysis must be strongly correlated, and, in fact, it is not possible to carry out such analysis closer than about 70 °C below T_0. Of course, our analysis indicates the presence of two modes. Our point here is simply that it is not possible to draw the same conclusion from the Raman spectra alone near T_0.

When a mode with a strong-scattering cross section (e.g., the LA mode) couples a weakly scattering mode (e.g., the "missing" soft mode), intuition suggests that the latter should acquire significant intensity if the spectral profiles of the two modes overlap. At first glance, it would appear that there is a contradiction, since the missing soft mode should then become quite obvious in the spectrum. To investigate this point we have considered the spectral profile of the scattered light within the bilinear coupling model. Since the dominant coupling near T_0 is the soft component Ω_1, we shall for simplicity consider only that coupling in what follows. The scattered spectrum is given in general for two coupled modes by the expression[22]

$$S(q,\omega)=-\frac{(n+1)}{\pi}\mathrm{Im}\sum_{ij=a,s}F_iF_j\chi_{i,j}(q,\omega)\ , \tag{6}$$

where n is the occupation number for an excitation of energy $\hbar\omega$, the F_i represent the scattering strengths of the uncoupled modes, and the generalized susceptibility components χ_{ij} are given by

$$\chi_{i,j}=\frac{\chi_i}{1-K^2\chi_a\chi_s}$$

and

$$\chi_{as}=\frac{K\chi_a\chi_s}{1-K^2\chi_a\chi_s}\ ,$$

where the $\chi_{a,s}$ represent the uncoupled susceptibilities of the acoustic and soft modes, respectively. The uncoupled susceptibilities are described by damped harmonic oscillators

$$\begin{aligned}\chi_a&=(\omega^2-\omega_a^2+2i\omega\gamma_a)^{-1}\ ,\\ \chi_s&=(\omega^2-\Omega_1^2+2i\omega\Gamma_1)^{-1}\ ,\end{aligned} \tag{7}$$

where the parameters ω_a, Ω_1, γ_a, and Γ_1 are independent of frequency. For our case, we wish to see if the soft mode would acquire scattering intensity from the acoustic mode due to this coupling. Hence, in order to investigate this, we shall set $F_3=0$, and inspect only χ_{aa} in Eq. (6). The expression for χ_{aa} given above may be written as a damped-harmonic-oscillator function (7) with frequency-dependent frequency and damping parameters

$$\omega'^2_a=\omega_a^2-\frac{K^2(\Omega_1^2-\omega^2)}{(\Omega_1^2-\omega^2)^2+4\omega^2\Gamma_1^2}\ ,$$
$$\Gamma'_{1a}=\gamma_a+\frac{K^2\Gamma_1/2}{(\Omega_1^2-\omega^2)^2+4\omega^2\Gamma_1^2}\ . \tag{8}$$

For the modes under consideration here, we easily identify

$$K=q\eta_0(K_2+K_3)\sin\phi_0/(m^*\rho)^{1/2}$$

from the behavior of C_{11} [Eq. (4), $K_4\sim 0$], and using the fact that $\omega_a^2=q^2C_{11}/\rho$, where ρ is the mass density. It can be shown by simple algebraic analysis that no peak is evident in the spectral response due to the term χ_{aa} when the soft mode is overdamped and located at frequencies significantly above ω'_a and γ'_a. This conclusion is also supported by calculations which we have performed for the parameter values extracted from the fit which show that even very near T_0 the deviation of the line shape from that of a simple damped harmonic oscillator is well within the experimental noise. Hence, the experimental observations are in fact consistent with the model given above.

As a byproduct of this analysis, as noted above, we obtain a measure of the optic-mode damping Γ_1 from the values of γ'_a by using Eq. (8). These values are also displayed in Fig. 10(a) for the temperature range where unambiguous determination is possible. These values lie quite far below the values extracted from an earlier two-mode analysis of the Raman spectrum at much lower temperatures.[5] However, since the latter analysis is based on decomposition of two strongly overlapping peaks in the Raman spectrum and ours incorporates new data (i.e., the observed values of γ'_a) we believe the present determination to be more reliable. Since the soft mode is apparently a very weak scatterer, the values are consistent with the observed Raman spectra.

Despite the success of the preceding analysis, it remains somewhat unsatisfactory to postulate the existence of a mode which has never been unambiguously observed. In view of these considerations, we must emphasize that our model is a tentative one and will remain so until unambiguous independent evidence can be obtained for the existence of the soft mode Ω_1.

In summary, then, we have the following answers to the problems posed in the Introduction. Our search at high resolution and high contrast for evidence of a very-low-frequency mode showed no evidence of such a feature, either overdamped or propagating. From careful study of the Raman and Brillouin spectra we have shown that in order to account for the anomalies in the elastic properties of the crystals within the context of the free energies which have been derived theoretically it is necessary to postulate the existence of a soft-mode branch which is similar to that postulated by other workers.[8,14] By using the complete free-energy expression (2), taking into account the fact that the static distortion and the soft-mode eigenvectors are not simply related, we have obtained a fit which simultaneously describes all the available acoustic data. We have also concluded that the lack of scattering intensity for the "unseen" optic mode is consistent with the failure of our high-contrast attempts to observe it, if its intrinsic scattering intensity is negligible. However, we have emphasized that in the absence of an unambiguous direct observation of the mode our interpretation remains tentative. Our high-resolution measurements of the Brillouin line shape provide determinations of the acoustic damping, which in turn allow us to extract soft-mode damping parameters in the context of the proposed model. There is substantial disagreement between these values and the extrapolation of those inferred by Shigenari *et al.*[8] Further, our search for central peak scattering in TMO has shown no evidence for such a mode with observable intensity outside $\pm 0.02\ \mathrm{cm}^{-1}$.

Finally, we emphasize again the need for theoretical understanding of the most striking anomaly near T_0: The singularity in the *damping* of the optic mode observed in the Raman spectrum with the concomitant increase in the Brillouin width. There is at present no theoretical explanation for such a strong anomaly in that damping, especially in the case of the branch which does not soften.

ACKNOWLEDGMENTS

We are pleased to acknowledge many helpful conversations of the results with H. Z. Cummins and W. Yao, and we are also grateful for a preprint of their results which they provided us prior to the publication of Ref. 14. We thank T. J. Negran and H. L. Carter for experimental assistance, and A. M. Glass for helpful comments on the manuscript.

APPENDIX: THE FREE-ENERGY EXPANSION

In this appendix we give the details of the derivation of the tilt angle between the order-parameter axes and the axes of the free-energy ellipsoid. The fact that dynamical variables and the static distor-

tion are not collinear in the low-temperature phase leads us to include additional terms in the free-energy expansion (2) resulting in a somewhat different form for the free energy related to the interaction of the acoustic and soft modes of the system. Since this derivation forms the basis for our conclusion that the static distortion is not collinear with either dynamic variable in the low-temperature phase, it forms an important link in our argument. The plan of our approach is as follows. We shall write the free energy in the (η_1,η_2) plane, where the η_i are the coordinates of an orthogonal representation of the order-parameter space. That is, the magnitude of the order parameter is given by $\eta_0^2=\eta_1^2+\eta_2^2$. We then find the condition that the major and minor axes of the equipotential surfaces near a minimum lie along the coordinate axes. Using this condition, we fix the coordinates by an appropriate choice of free-energy parameters and solve for the position of the static order parameter value below T_0.

It is convenient to visualize the curve generated by the intersection of the free-energy surface $F(\eta_1,\eta_2)$ and the plane $F=F_c$. If F_c is near the free-energy minimum F_0 at $\vec{\eta}_0$ then this curve will be roughly an ellipse in the (η_1,η_2) plane. An ellipse with its axes a and b along the coordinate axes x and y may be represented by the form $c=x^2/a^2+y^2/b^2$, where c is another positive constant. Any cross term between x and y in this form represents a tilt of the axes with respect to the coordinates. Thus, if we expand the free energy about a minimum at $\vec{\eta}_0$,

$$F(\vec{\eta})=F_0+\frac{\partial^2 F}{\partial\eta_1^2}\delta\eta_1^2+\frac{\partial^2 F}{\partial\eta_2^2}\delta\eta_2^2+\frac{\partial^2 F}{\partial\eta_1\partial\eta_2}\delta\eta_1\delta\eta_2\ , \tag{A1}$$

then the condition that the major and minor axes lie along the coordinates is just that the last term be zero. That is, we require that

$$\frac{\partial^2 F}{\partial\eta_1\partial\eta_2}=0 \tag{A2}$$

at $\vec{\eta}=\vec{\eta}_0=(\eta_{10},\eta_{20})$. In addition, there is the implicit condition that we are expanding around an extremum, which may be expressed as

$$\frac{\partial F}{\partial\eta_1}=\frac{\partial F}{\partial\eta_2}=0\ . \tag{A3}$$

We now use these conditions in discussing the free energy form proposed by Dorner *et al.*[4] [their Eq. (10), as modified by Eq. (14)], where the portion relevant to our concerns here is

$$F=\tfrac{1}{2}\omega_M^2\eta^2+\tfrac{1}{4}\sum_\alpha B_\alpha f_\alpha^{(4)}(\eta_i)+\tfrac{1}{6}\sum_\alpha W_\alpha f_\alpha^{(6)}(\eta_i)+\cdots\ , \tag{A4}$$

and we have converted their notation (γ_i) to ours by the substitution $\eta_i\equiv\eta_0\gamma_i$. The functions represented by the sums are given by

$$\sum_\alpha B_\alpha f_\alpha^{(4)}(\eta_i)=B_1(\eta_1^4+\eta_2^4)+2B\eta_1^2\eta_2^2+4B_3(\eta_1^2-\eta_2^2)\eta_1\eta_2$$

and

$$\sum_\alpha W_\alpha f_\alpha^{(6)}(\eta_i)=W_1(\eta_1^6+\eta_2^6)+3W_2(\eta_1^2+\eta_2^2)\eta_1^2\eta_2^2+6W_3(\eta_1^2+\eta_2^2)(\eta_1^2-\eta_2^2)\eta_1\eta_2\ .$$

Constructing the derivatives of this free-energy function in order to apply the conditions (A2) and (A3) is a straightforward, albeit intricate, procedure. It turns out, however, that the condition (A3) may be ignored for our purposes here, since the condition (A2) yields the requisite information, as follows. Constructing the cross derivative and then making the substitutions $\eta_1=\eta_0\sin\phi$ and $\eta_2=\eta_0\cos\phi$, we obtain the condition

$$B_2\eta_0^2\sin2\phi_0-3B_3\eta_0^2\cos2\phi_0+2W_2\eta_0^4\sin2\phi_0-5W_3\eta_0^4\cos2\phi_0=0\ , \tag{A5}$$

which immediately yields the solution

$$\tan2\phi_0=\frac{3B_3+5W_3\eta_0^2}{B_2+2W_2\eta_0^2}\ .$$

Note that in writing Eq. (A5) in terms of η_0 we have implicitly assumed that it is evaluated at the position of the minimum defined by Eq. (A3). The value of ϕ_0 which results from this treatment gives the orientation of that equilibrium position from the origin in the coordinate system defined by (A2) such that the axes are parallel to the major and minor axes of the equipotential ellipse. Alternatively then, if we change coordinates so that that minimum falls on an axis (as is normally done) then the equipotential ellipse will be tilted by an angle $-\phi_0$, which is just the complement of the angle ψ defined by Yao *et al.*[14] and referred to in our discussion before Eq. (1).

Finally, we emphasize that a nonzero value of ϕ_0 does not imply a nonzero value for K_4, as discussed after Eq. (4) in the text. In that discussion, we have used an approximate treatment of the free-energy

expansion analogous to that given above, to argue that choosing the axes such that they are parallel to the dynamic variable eigenvectors is in fact nearly equivalent to setting K_4 to zero. Yao *et al.*[14] choose coordinates by setting $K_4 \equiv 0$, and then, using equations derived for the condition $\vec{\eta}_0 = (\eta_0, 0)$, they found that the dynamic variables were tilted with respect to those axes. In fact, the two conditions placed on the coordinates in this fashion are incompatible, and in the present treatment we find that the coordinate systems defined by the dynamic variables and by the condition $K_4 \equiv 0$ practically coincide, while that defined by the condition $\vec{\eta}_0 = (\eta_0, 0)$ is rotated significantly with respect to the first two. According to our fits to the data, we find that the rotation angle is $\phi_0 = 76°$.

In concluding this appendix, we note that similar considerations may apply in the case of other structural phase transitions with multidimensional order parameters, where it has usually been assumed that the static distortion is proportional to the eigenvector of one of the dynamic modes in the low-symmetry phase. The present discussion makes it clear that such is not always the case, and that taking these effects into account may significantly alter the interpretation of experimental data.

---

*On leave from University of Campinas, Brazil.

[1]H. J. Bochardt and P. E. Bierstedt, Appl. Phys. Lett. 8, 50 (1966).
[2]L. E. Cross, A. Fouskova, and S. E. Cummins, Phys. Rev. Lett. 21, 812 (1968).
[3]W. Jeitschko, Acta Crystallogr., Sect. B 28, 60 (1972); S. C. Abrahams, C. Svensson, and J. L. Bernstein, J. Chem. Phys. 72, 4278 (1980).
[4]B. Dorner, J. D. Axe, and G. Shirane, Phys. Rev. B 6, 1950 (1972).
[5]P. A. Fleury, Solid State Commun. 8, 601 (1970).
[6]J. Petzelt, Solid State Commun. 9, 1485 (1971).
[7]Q. Kim and F. G. Ullman, Phys. Rev. B 18, 3579 (1978).
[8]T. Shigenari, Y. Takagi, and Y. Wakabayashi, Solid State Commun. 18, 1271 (1976).
[9]J. M. Courdille, R. Deroche, and J. Dumas, J. Phys. (Paris) 36, 891 (1975).
[10]B. A. Agishev, S. K. Esayan, V. V. Lemanov, and T. M. Polkhouskaya, Fiz. Tverd. Tela (Leningrad) 20, 3480 (1978) [Sov. Phys.—Solid State 20, 2012 (1978)].
[11]Y. Luspin and G. Hauret, Phys. Status Solidi B 76, 551 (1976).
[12]U. T. Höchli, Phys. Rev. B 6, 1814 (1972).
[13]S. K. Esayan, B. D. Laikhtman, and V. V. Lemanov, Zh. Eksp. Teor. Fiz. 68, 689 (1975) [Sov. Phys.—JETP 41, 342 (1975)].
[14]W. Yao, H. Z. Cummins, and R. H. Bruce, Phys. Rev. B 24, 424 (1980).
[15]K. B. Lyons and P. A. Fleury, J. Appl. Phys. 47, 4898 (1976).
[16]A. M. Glass, M. E. Lines, F. S. L. Hsu, and H. J. Guggenheim, Ferroelectrics 22, 701 (1978).
[17]S. Itoh and T. Nakamura, Phys. Lett. 44A, 461 (1973).
[18]E. Pytte, Solid State Commun. 8, 2101 (1970).
[19]V. Dvorak, Phys. Status Solidi B 45, 147 (1971); J. Petzelt and V. Dvorak, Phys. Status Solidi B 46, 413, 763 (1971).
[20]A. P. Levanyuk and D. G. Sannikov, Fiz. Tverd. Tela (Leningrad) 12, 2997 (1970) [Sov. Phys.—Solid State 12, 2418 (1971)].
[21]S. E. Cummins, Ferroelectrics 1, 11 (1970).
[22]P. Fleury, Comments Solid State Phys. 4, 167 (1972).